Petrography of volcaniclastic rocks in intra-arc volcano-bounded to fault-bounded basins of the Rosario segment of the Lower Cretaceous Alisitos oceanic arc, Baja California, Mexico

K.M. Marsaglia [a,*], M. Barone [b], S. Critelli [b], C. Busby [c], B. Fackler-Adams [d]

[a] Department of Geological Sciences, California State University Northridge, 18111 Nordhoff St, Northridge, CA 91330-8266, USA
[b] Dipartimento di Biologia, Ecologia e Scienze della Terra, Università degli Studi della Calabria, I-87036 Arcavacata di Rende (CS), Italy
[c] Department of Earth and Planetary Sciences, University of California, Davis, CA 95616, USA
[d] Skagit Valley College, 2405 E. College Way, Mount Vernon, WA 98273, USA

ARTICLE INFO

ABSTRACT

The Rosario segment of the Early Cretaceous Alisitos oceanic magmatic arc in Baja California displays a record of arc-axis sedimentation and volcanism that is well preserved in outcrops within a southern volcano-bounded and a northern fault-bounded basin that flanked an intervening subaerial edifice. This record includes volcanic and volcaniclastic rocks that range from felsic to mafic in composition. Volcaniclastic/tuffaceous sandstone samples from two previously published measured sections are mainly composed of volcanic clasts with moderate plagioclase content. Locally quartz and/or potassium feldspar are present in trace to moderate amounts. The proportions of volcanic lithic types exhibiting vitric, microlitic, lathwork, and felsitic textures are highly variable with no distinct stratigraphic trends, likely as a function of the mixed styles of eruption and magma compositions that produced pyroclasts, as well as erosion-produced epiclastic debris. The volcaniclastic fill of the basins is consistent with an oceanic arc setting, except for the relatively high felsitic volcanic lithic content, likely associated with subaerial, as opposed to the more common submarine felsic magmatism associated with arc extension in oceanic settings. There are no major differences in compositional modes of tuff and sandstone between the fault-bounded and volcano-bounded basin strata, even though they exhibit distinctly different volcaniclastic facies. This suggests that proximal arc-axis basins of varying types around a single major subaerial edifice provide a faithful record of volcanic trends in the arc segment, regardless of variation in transport and depositional processes.

© 2015 Elsevier B.V. All rights reserved.

1. Introduction

Intra-arc basins can be discriminated from forearc and backarc basins in the rock record partly on the presence of arc-axis volcanic and related intrusive rocks (e.g., Smith and Landis, 1995). Smith and Landis (1995) classified intra-arc basins on the arc platform as volcano-bounded or fault-bounded, the former being bordered by constructional volcanic edifices and the latter bounded by normal or oblique-slip faults. They also discussed hybrid varieties with aspects of both types. Previous workers have contrasted compositional modes of volcaniclastic successions associated with forearc and backarc basins, as well as nascent backarc basins (e.g., Dickinson and Suczek, 1979; Dickinson et al., 1983; Marsaglia, 1992; Marsaglia and Ingersoll, 1992; Marsaglia and Devaney, 1995; Critelli et al., 2002; Caracciolo et al., 2011; Cavazza et al., 2013), but none has examined compositional differences in proximal basins along the arc axis, where drilling recovery in modern settings is limited (Marsaglia, 1995).

This paper compares volcaniclastic compositional modes of samples taken from a shallow-marine volcano-bounded basin and a largely deep-marine fault-bounded basin on either side of a subaerial edifice, along a 60 km-long segment of the Alisitos arc mapped in detail by Busby et al. (2006), in Baja California, Mexico (Fig. 1). The fill of these two basin types contrasts markedly in volcanic and volcaniclastic lithofacies, reflecting differing transport and depositional processes in the two basins types, as shown by detailed maps and measured sections (Busby et al., 2006), and discussed further below. We show in this paper that despite the differences in basin types and associated transport and depositional processes, the detrital modes do not vary significantly, suggesting that proximal arc-axis basins of varying types around a single major subaerial edifice provide a faithful record of volcanic trends in the arc segment, regardless of transport and depositional processes.

* Corresponding author.
    E-mail addresses: kathie.marsaglia@csun.edu (K.M. Marsaglia), bamirko@libero.it (M. Barone), salvatore.critelli@unical.it (S. Critelli), cjbusby@ucdavis.edu (C. Busby), Ben.Fackler-Adams@skagit.edu (B. Fackler-Adams).
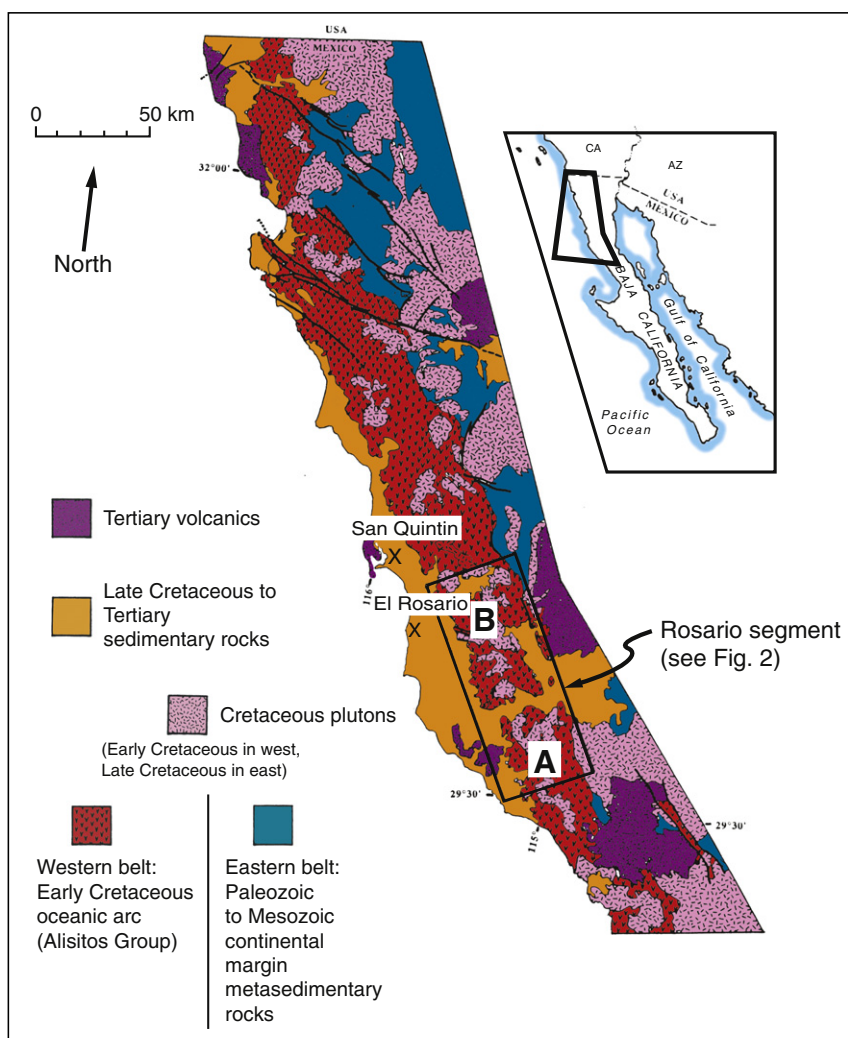
Fig. 1. Location map of study area from Busby et al. (2006) showing the regional geologic setting of the Alisitos arc with respect to the western Peninsular Ranges of Baja California, Mexico. The positions of measured sections shown in Fig. 2 are marked at "A" and "B."

2. Previous work

Development of the Alisitos extensional oceanic arc (ca. 140–100 Ma) was preceded by, and is partly floored by, strongly extensional oceanic arc-ophiolite systems (ca. 220–130 Ma), including the Gran Canon Formation of Cedros Island (Busby, 2004). Together, these oceanic arc terranes were accreted to the Mexican margin at 105–100 Ma, where ongoing subduction produced a high-standing continental arc (ca. 100–50 Ma) that lies to the east of the accreted oceanic arc rocks. The stratigraphy of the Gran Canon Formation was interpreted to record rifting of an oceanic arc to form a backarc basin undergoing seafloor spreading, followed by progradation of a backarc apron onto a backarc seafloor spreading center (Busby and Boles, 1988; Busby-Spera, 1988). Later work on detrital modes of volcaniclastic/tuffaceous sandstones demonstrated a second arc rifting event, recorded by silicic pyroclastic flows and mafic lavas, typical of extension in modern oceanic arcs such as the Izu–Bonin arc (Taylor et al., 1990); this was followed by epiclastic sedimentation in the newly formed remnant arc basin (Critelli et al., 2002). Herein, we report petrographic data from the Rosario segment of the oceanic extensional Alisitos arc (Fig. 1; Busby et al., 2006), using similar techniques, with a similar goal of elucidating this later phase of magmatic-arc history, as well as comparing and contrasting compositional modes in a volcano-bounded and a fault-bounded basin on either side of a subaerial edifice along the arc axis.

The Early Cretaceous Alisitos arc crops out extensively along the western half of Baja California Norte, in a belt 30 km wide and 300 km long (Fig. 1). The geologic history of the Alisitos arc is closely related to that of the Mexican mainland for the same time frame (Wetmore, 2002; Wetmore et al., 2003; Centeno-Garcia et al., 2011). The Alisitos arc (also referred to as Alisitos Group) consists of dominantly intermediate-composition volcanic and volcaniclastic rocks, and lesser mafic and silicic volcanic rocks, with abundant marine fossils, and associated hypabyssal and plutonic rocks (Silver et al., 1963; Fackler-Adams and Busby, 1998; Busby, 2004; Busby et al., 2006). The Alisitos arc was accreted to the North American plate at about 110–100 Ma (e.g., Dickinson and Lawton, 2001; Busby, 2004; Alsleben et al., 2012). Recent publications have provided more detail regarding arc evolution by focusing on the plutonic rock record in Baja California (Morton and Miller, 2014, and papers therein).

U-Pb zircon dates on volcanic and plutonic rocks of the Rosario segment of the Alisitos arc (Figs. 1, 2) indicate that the entire 4 km-thick upper to middle crustal section formed in only 1.5 million years, at ~111–110 Ma, in an extensional environment (Busby et al., 2006). Superior exposure, widespread pyroclastic units, and a lack of post-volcanic deformation in the Rosario segment of the Alisitos arc allowed Busby et al. (2006) to divide its 1.5 my of growth into four time slices, grouped into two tectonic phases (Fig. 2). Phase 1 (time slices 1 through 3, Fig. 2) constitutes over three-fourths of the stratigraphic section and consists of intermediate to silicic lava flows, lava domes, and primary
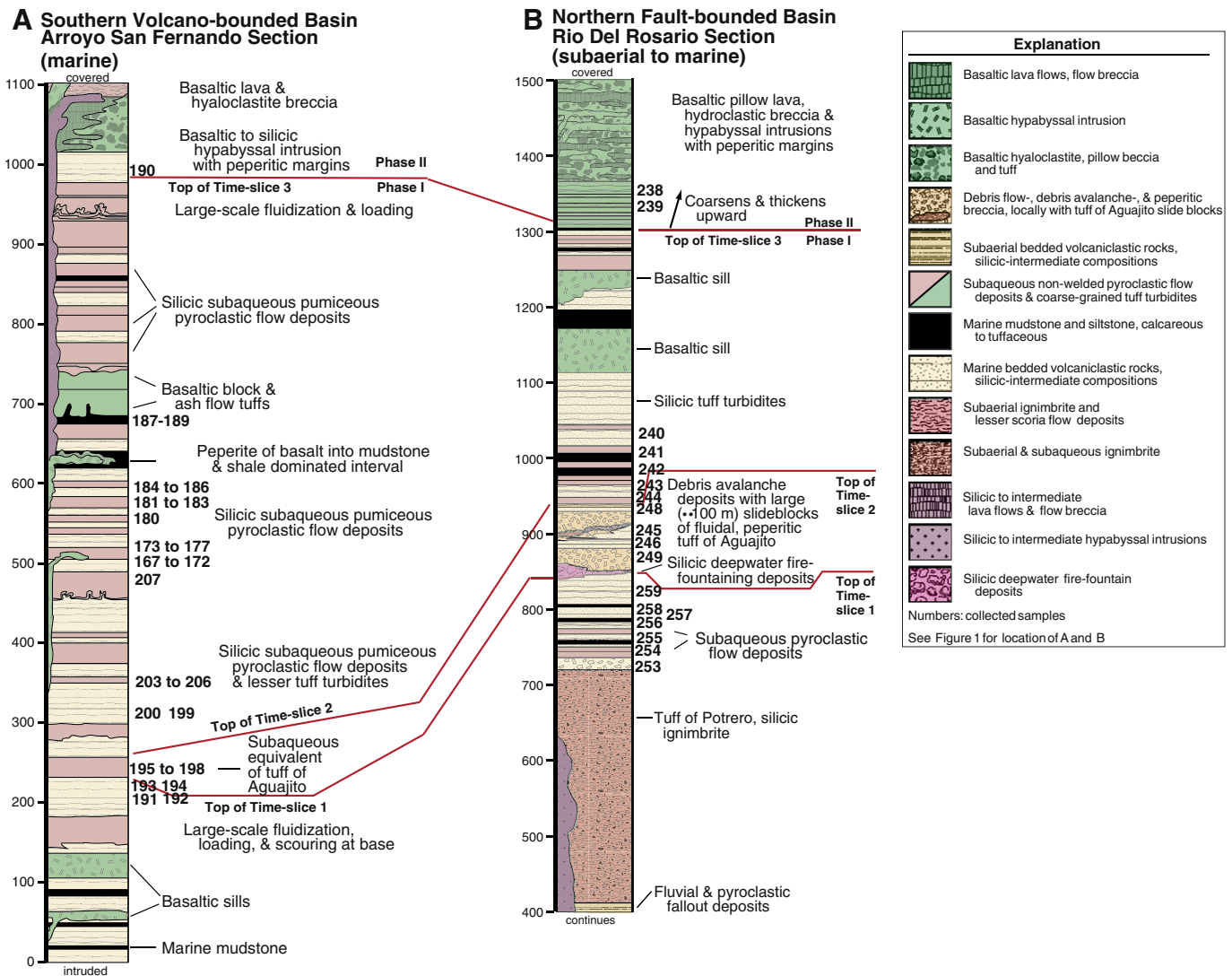
Fig. 2. Stratigraphic columns for volcano-bounded basin (A) and fault-bounded basin (B) in the Rosario segment of the Alisitos arc (from Busby et al., 2006); time-slice correlations (shown in red) made by detailed mapping across the 60 km-long arc segment, shown in Busby et al. (2006). This figure is modified to show positions of samples described in this paper.

and reworked pyroclastic deposits, with widespread vent facies. Stage 1 was referred to as an "extensional arc," owing to the presence of syndepositional normal faults, high rates of subsidence (>1 km/my), and the presence of two silicic calderas and granitic underpinnings (Busby et al., 2006). Phase 2 (time slice 4), which constitutes the uppermost ~25% of the exposed stratigraphic section (Fig. 2), consists of widespread mafic lava flows, hyaloclastites, mafic tuffs, and reworked mafic debris, fed by abundant mafic dikes that pass downward into plutons (Busby, 2004; Busby et al., 2006). Phase 2 was interpreted to record an episode of arc rifting. Thus the Rosario segment of the Alisitos oceanic arc records the arc rifting.

3. Sampling strategy

For the current study, we collected samples from a stratigraphic section through the southern volcano-bounded basin (Fig. 2A), which is dominantly shallow-marine facies, and from the northern fault-bounded basin (Fig. 2B), which is dominantly deep-marine facies, except for a basal fluvial section beneath a marine caldera-filling silicic ignimbrite (Fig. 2; Busby et al., 2006). These basins have a higher proportion of well-stratified sand than the intervening subaerial edifice,

which is dominated by more coherent lavas and massive pyroclastic flow deposits, some welded (Busby et al., 2006).

The structure and stratigraphic architecture of the two types of basin differs in several significant ways (Busby et al., 2006). The northern fault-bounded deep-marine basin was bounded to the south by the rugged, faulted northern flank of the subaerial edifice; mass wasting deposits were shed into the deepwater basin from the faulted flank (e.g., debris avalanche deposits, Fig. 2B), and pyroclastic flows that entered this basin across the steep margin disintegrated into turbidity currents, forming well-stratified, well-sorted deposits, ranging from monomictic ("tuffaceous turbidites") to mixed silicic-intermediate compositions ("bedded volcaniclastic rocks," Fig. 2B). In contrast, the southern shallow-marine volcano-bounded basin (Fig. 2A) had gentler slopes on the flanks of the central subaerial edifice to the north, thereby supporting extensive biohermal buildups (Busby et al., 2006) and allowing pyroclastic flows to enter the basin with greater integrity, producing thick, poorly sorted, poorly stratified, monomictic deposits (subaqueous pyroclastic flow deposits), interstratified with well-stratified rocks of mixed silicic-intermediate composition ("tuff turbidites," Fig. 2A). Despite these differences in transport and depositional processes, most of the samples in this study were taken from a part of the section inferred to be sourced from the central subaerial edifice (Busby

et al., 2006), except for the mafic tuffs at the top of deepwater fault-bounded basin (samples 238 and 239, Fig. 2B). In this paper, we compare samples in the two basin types to determine if the contrast in basin structure and transport and depositional processes is reflected in detrital modes. We also sampled, to evaluate the proportion of primary pyroclastic particles (mainly glass) and the epiclastic volcanic debris, directly erupted from *vs.* eroded from the central subaerial edifice via stream or coastal processes.

4. Methods

Intervals dominated by sand components (tuffaceous/volcaniclastic sandstones and tuffs) from the two stratigraphic sections were sampled (Fig. 2). Thin sections were prepared, etched with hydrofluoric acid, and stained for feldspar recognition. The samples have undergone relatively minor zeolite-grade metamorphism/alteration, with some textural modification. Fifty-five of the least-altered tuffaceous/volcaniclastic sandstone and tuffs were petrographically analyzed, 37 from the volcano-bounded marine basin section and 18 fault-bounded marine basin section (Fig. 2). The Gazzi–Dickinson method of point counting (Ingersoll et al., 1984) was used so that results could be compared with previously collected data sets from other intraoceanic arc settings (e.g., Marsaglia, 1992; Marsaglia and Devaney, 1995; Marsaglia and Ingersoll, 1992; Critelli et al., 2002). Point-count categories and recalculated parameters are defined in Table 1. Detrital modes are provided in Table 2. Point counting included detailed petrographic classes of volcanic particles using criteria defined by Marsaglia and Ingersoll (1992), Marsaglia (1993), Critelli and Ingersoll (1995), and Critelli et al. (2002).

Note that in this scheme, the term "lithic" is not used in the volcanological sense (non-vitric volcanic component), but as a sandstone petrologist would use it in a non-genetic sense to refer to sand grains

Table 1
Counted and recalculated parameters.

Qp:	Polycrystalline quartz
Qm:	Monocrystalline quartz
P:	Plagioclase
K:	Potassium feldspar
Lvu:	Volcanic lithic fragment undifferentiated
Lvv:	Vitric volcanic lithic
Lvf:	Felsitic vitric
Lvmi:	Microlitic vitric with fresh glass and plagioclase microlites
Lvl:	Lathwork vitric with plagioclase laths
Lm:	Metamorphic lithic fragment
Ls:	Sedimentary lithic fragment

$Qt = Qp + Qm$
$F = P + K$
$L = Lm + Ls + Lv$
$Lt = Lm + Ls + Lv + Qp$
$Lv = Lvu + Lvv + Lvmi + Lvl + Lvf$
$QtFL\%Q = 100 * Qt/(Qt + F + L)$
$QtFL\%F = 100 * F/(Qt + F + L)$
$QtFL\%L = 100 * L/(Qt + F + L)$
$QmFLt\%Qm = 100 * Qm/(Qm + F + Lt)$
$QmFLt\%F = 100 * F/(Qm + F + Lt)$
$QmFLt\%Lt = 100 * Lt/(Qm + F + Lt)$
$QmKP\%Qm = 100 * Qm/(Qm + K + P)$
$QmKP\%K = 100 * K/(Qm + K + P)$
$QmKP\%P = 100 * P/(Qm + K + P)$
$LvLmLs\%Lv = 100 * Lv/(Lv + Lm + Ls)$
$LvLmLs\%Lm = 100 * Lm/(Lv + Lm + Ls)$
$LvLmLs\%Ls = 100 * Ls/(Lv + Lm + Ls)$
$LvvLvmiLvl\%Lvv = 100 * Lvv/(Lvv + Lvmi + Lvl)$
$LvvLvmiLvl\%Lvmi = 100 * Lvmi/(Lvv + Lvmi + Lvl)$
$LvvLvmiLvl\%Lvl = 100 * Lvl/(Lvv + Lvmi + Lvl)$
$LvfLvmiLvl\%Lvv = 100 * Lvf/(Lvf + Lvmi + Lvl)$
$LvfLvmiLvl\%Lvmi = 100 * Lvml/(Lvf + Lvmi + Lvl)$
$LvfLvmiLvl\%Lvl = 100 * Lvl/(Lvf + Lvmi + Lvl)$

of volcanic origin (pyroclastic to epiclastic) exhibiting vitric, microlitic, lathwork, or felsitic textures. Other lithic clast types include metamorphic and sedimentary varieties, albeit these are rare in the Alisitos samples. Grain rounding and sorting were noted in descriptions but not quantitatively evaluated.

5. Results

The Alisitos samples are primarily composed of volcanic lithics (average Qt-F-L% = 2-19-79, with lithics including glass, as noted above), with lesser quartz and feldspar (Figs. 3, 4). The samples range from poorly sorted (matrix-supported texture) to moderately to well-sorted (grain-supported texture), with more poorly sorted samples containing mostly angular fragments, and better-sorted samples dominated by or including well-rounded grains (Fig. 4). Bioclasts, locally rounded, include mollusk, rudist, and echinoid fragments (Fig. 4A).

The monocrystalline components occur as sand-sized phenocrysts in lithic fragments and individual grains (Figs. 4B, C, D, 5). They are mainly plagioclase (ave. QmKP%P = 94) with minor quartz (ave. QmKP%Q = 5) and lesser potassium feldspar (ave. QmKP%K = 1). The quartz occurs as monocrystalline to polycrystalline grains. Plagioclase crystals as phenocrysts in lithic clasts exhibit euhedral to subhedral habits and are locally twinned and zoned. Ten of the samples contain trace to minor amounts of potassium feldspar (Table 2), with some tabular crystals displaying carlsbad twinning.

The lithic fraction is largely dominated by volcanic lithics (ave. LmLvLs%Lv = 99) with very minor amounts of sedimentary and metamorphic lithic components, the latter only in the northern fault-bounded basin section, presumably shed from rocks deformed along the fault (Figs. 4, 6). Glass alteration precluded collecting detailed information on the proportions of colorless vs. brown glass, but despite alteration/dissolution diagnostic textures are preserved. The volcanic lithics exhibit a range of holocrystalline to microcrystalline to vitric textures and were classified accordingly as vitric, microlitic, lathwork, and felsitic volcanic lithic components (e.g., Dickinson, 1970; Fig. 4B, C, D). The vitric fragments are variably vesicular. The proportions of these volcanic textures are highly variable from sample to sample, with lathwork (Lvl) textures being the least common (Figs. 7, 8). The volcanic lithics are dominantly neovolcanic (glass) varieties according to the criteria proposed by Critelli and Ingersoll (1995), indicating that they are largely pyroclastic (not epiclastic) in origin, but where rounded, the glassy fragments were likely reworked by waves or currents prior to deposition (Fig. 4D). Some samples appear to be more mafic (e.g. samples 233, 249, 246, 204, and 174) in that they contain black tachylitic glass, a likely product of subaerial volcanism (see Marsaglia (1993) for discussion) that is relatively stable under diagenetic conditions (see discussion in Critelli et al., 2002). Other samples have high proportions of microcrystalline felsitic fragments, which are characteristic erosion products of subaerial felsic volcanism (see discussion in Marsaglia, 1991). The metamorphic lithic fragments are mainly phyllite and the sedimentary rock fragments include mudstone (rip-up clasts?), and micritic to sparry limestone fragments.

Even though the volcaniclastic rocks of the Alisitos Formation are variably altered, they retain significant provenance information as deduced in similar volcaniclastic rocks (Marsaglia, 1991; Marsaglia and Tazaki, 1992; Perri et al., 2012). Only a few samples where alteration blurred grain boundaries were excluded from the study. The glassy components are largely dissolved and replaced by authigenic phases except for the mafic tachylitic volcanic fragments mentioned above. Therefore, inferences on magma chemistry from translucent glass color, e.g., colorless felsic and tan/brown intermediate to mafic (Marsaglia, 1992), are not possible. Volcanic lithic fragments are variably altered to clay minerals (smectite?), chlorite, sericite, carbonate, silica, and zeolites, and some exhibit devitrification textures. Altered feldspar and dense-mineral phenocrysts are mostly replaced by carbonate, and as glass more readily dissolves than phenocrysts, the carbonate
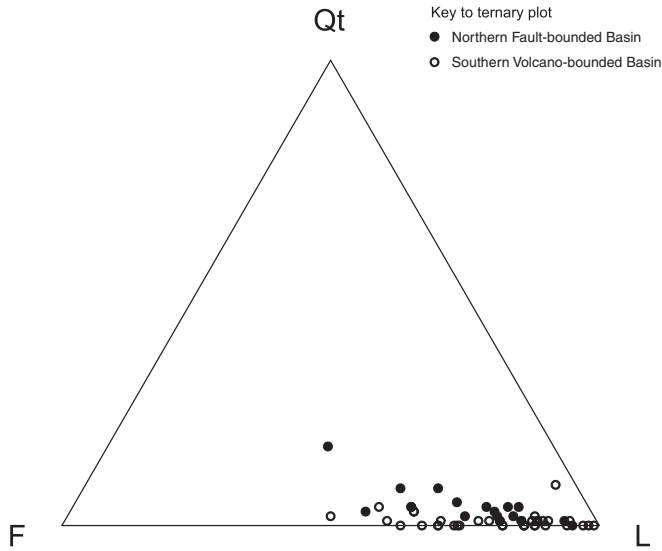
Table 2
Compositional modes.

| Stratigraphic section/sample no.	Qm	F	Lt	Qt	F	L	Qm	K	P	Lm	Lv	Ls	Lvv	Lvmi	Lvl	Lvf	Lvmi	Lvl	Lv/L	P/F
	%			%			%			%			%			%				
Arroyo San Fernando (ASF)																				
95-SC-190	7	23	70	7	3	70	23	4	73	0	100	0	*primary tuff*			—	—	—	—	—
95-SC-189	1	20	79	1	20	79	2	0	98	0	100	0	0	51	49	30	45	44	—	—
95-SC-188	0	14	86	0	14	86	0	0	100	0	100	0	0	71	29	2	70	28	—	—
95-SC-187	4	33	63	4	33	63	11	0	89	0	97	3	0	42	58	7	39	54	—	—
95-SC-186	0	10	90	0	10	90	0	0	100	0	100	0	0	59	41	14	31	55	—	—
95-SC-185	0	12	88	0	12	88	0	0	100	0	100	0	19	48	33	16	40	44	—	—
95-SC-184	0	27	73	0	27	73	0	0	100	0	100	0	25	61	14	24	62	14	1.00	1.00
95-SC-183	0	33	67	0	33	67	0	19	81	0	100	0	2	50	48	12	45	43	—	—
95-SC-182	0	30	70	0	30	70	1	0	99	0	100	0	13	58	29	46	36	18	—	—
95-SC-181	1	39	60	1	39	60	2	0	98	0	100	0	0	60	40	91	5	4	—	—
95-SC-180	1	11	88	1	11	88	8	0	92	0	100	0	6	83	11	15	75	10	1.00	1.00
95-SC-177	0	30	70	0	30	70	1	6	93	0	100	0	0	91	9	22	70	8	—	—
95-SC-176	0	1	99	0	1	99	17	0	83	0	100	0	73	26	1	0	98	2	1.00	1.00
95-SC-175	0	26	74	0	26	74	1	0	99	0	99	1	0	41	59	5	39	56	—	—
95-SC-174	0	2	98	0	2	98	0	0	100	0	100	0	95	4	1	0	87	13	1.00	1.00
95-SC-173	2	11	87	2	11	87	14	0	86	0	100	0	5	79	16	13	72	15	—	—
95-SC-172	1	10	89	1	10	89	8	0	92	0	100	0	60	40	0	99	1	0	1.00	1.00
95-SC-171	1	11	88	1	11	88	4	0	96	0	98	2	0	54	46	29	38	33	—	—
95-SC-170	1	14	85	1	14	85	5	0	95	0	100	0	5	57	38	82	11	7	1.00	1.00
95-SC-169	0	5	95	1	5	94	4	0	96	0	100	0	14	66	20	63	28	9	1.00	1.00
95-SC-168	0	6	94	0	6	94	0	0	100	0	99	1	20	51	29	81	12	7	0.99	1.00
95-SC-167	0	14	86	0	14	86	0	0	100	0	100	0	15	54	31	44	36	20	1.00	1.00
95-SC-207	0	28	72	0	28	78	0	8	92	0	100	0	47	44	9	81	16	3	1.00	1.00
95-SC-206	0	37	63	0	37	63	1	2	97	0	100	0	39	42	19	84	11	5	1.00	0.98
95-SC-205	1	29	70	1	29	70	4	3	93	0	100	0	72	26	2	94	6	0	1.00	0.93
95-SC-204	0	12	88	0	12	88	0	0	100	0	100	0	6	59	35	3	61	36	1.00	1.00
95-SC-203	2	49	49	2	49	49	5	11	84	0	100	0	72	14	14	98	1	1	1.00	0.88
95-SC-200	1	12	87	1	12	87	4	0	96	0	100	0	7	68	25	26	54	20	1.00	1.00
95-SC-199	0	18	82	0	18	82	2	0	98	0	100	0	33	37	30	87	7	6	1.00	1.00
95-SC-198	3	97	0	0	3	97	0	0	100	0	99	1	25	69	6	12	81	7	1.00	1.00
95-SC-197	3	33	64	3	33	64	8	0	92	0	100	0	4	77	19	10	72	18	1.00	1.00
95-SC-196	4	39	57	4	39	57	9	3	88	0	100	0	0	78	22	17	65	18	1.00	0.97
95-SC-195	1	9	90	1	9	90	8	0	92	0	100	0	29	63	8	26	65	9	1.00	1.00
95-SC-194	1	22	77	1	22	77	4	0	96	0	100	0	28	45	27	73	17	10	1.00	1.00
95-SC-193	0	14	86	0	14	86	2	0	98	0	100	0	33	33	34	77	11	12	1.00	1.00
95-SC-192	3	33	64	3	33	64	8	0	92	0	100	0	32	34	34	86	7	7	1.00	1.00
95-SC-191	0	18	82	0	18	82	0	0	100	0	100	0	0	74	26	4	71	25	1.00	1.00
Average	**1**	**22**	**76**	**1**	**19**	**79**	**4**	**2**	**94**	**0**	**100**	**0**	**22**	**53**	**25**	**41**	**41**	**18**	**1.00**	**0.99**
Standard deviation	**2**	**17**	**18**	**2**	**12**	**13**	**5**	**4**	**6**	**0**	**1**	**1**	**26**	**19**	**16**	**35**	**28**	**17**	**0.00**	**0.03**
Rio del Rosario (RDR)																				
95-SC-238	0	6	94	1	6	93	0	0	100	0	100	0	62	30	8	62	30	8	1.00	1.00
95-SC-239	2	15	83	2	15	83	10	0	90	0	100	0	64	28	8	93	5	2	1.00	1.00
95-SC-240	5	24	71	5	24	71	17	9	74	0	100	0	50	50	0	100	0	0	1.00	0.89
95-SC-241	3	33	64	4	33	63	7	0	93	0	75	25	67	33	0	99	1	0	0.75	1.00
95-SC-242	2	24	74	2	24	74	7	0	93	0	100	0	77	23	0	99	1	0	1.00	1.00
95-SC-243	3	15	82	4	15	81	16	0	84	0	100	0	42	21	37	86	5	9	1.00	1.00
95-SC-244	2	26	72	8	26	66	6	0	94	2	90	8	23	43	34	70	17	13	1.00	1.00
95-SC-248	6	33	61	8	33	59	15	0	85	0	84	16	91	9	0	99	1	0	0.84	1.00
95-SC-245	1	18	81	2	18	80	5	0	95	1	94	5	39	36	25	47	31	22	0.94	1.00
95-SC-246	0	5	95	0	5	95	0	0	100	0	100	0	21	55	24	12	61	27	1.00	1.00
95-SC-249	0	18	82	1	18	81	1	0	99	0	100	0	5	55	40	12	51	37	—	—
95-SC-259	3	19	78	4	19	77	14	0	86	0	100	0	60	16	24	97	1	2	1.00	1.00
95-SC-258	17	42	41	17	42	41	29	0	71	0	97	3	100	0	0	0	0	0	0.97	1.00
95-SC-257	3	18	79	3	18	79	13	0	87	0	98	2	2	25	73	3	24	73	0.98	1.00
95-SC-256	3	42	55	3	42	55	7	3	90	0	100	0	36	9	55	98	0	2	1.00	0.97
95-SC-255	1	14	85	1	14	85	6	0	94	0	100	0	0	84	16	87	11	2	1.00	1.00
95-SC-254	1	13	86	4	13	83	9	0	91	0	100	0	57	30	13	93	5	2	1.00	1.00
95-SC-253	1	18	81	1	18	81	3	0	97	0	99	1	0	100	0	93	7	0	0.99	1.00
Average	**3**	**21**	**76**	**4**	**21**	**75**	**9**	**1**	**90**	**0**	**97**	**3**	**44**	**36**	**20**	**73**	**15**	**12**	**0.97**	**0.99**
Standard deviation	**4**	**11**	**14**	**4**	**11**	**14**	**7**	**2**	**8**	**1**	**7**	**7**	**31**	**26**	**21**	**37**	**18**	**19**	**—**	**—**
Total average	**2**	**22**	**76**	**2**	**20**	**78**	**6**	**1**	**93**	**0**	**99**	**1**	**29**	**47**	**24**	**50**	**32**	**16**	**1**	**1**
Standard deviation	**4**	**11**	**14**	**4**	**11**	**14**	**7**	**2**	**8**	**1**	**7**	**7**	**31**	**26**	**21**	**37**	**18**	**19**	**0**	**0**

Note: samples are in roughly stratigraphic order.

may represent a late cementing phase. Authigenic titanite crystals are rare. Quartz and feldspar are also present as overgrowths, along with local epidote cement. The presence of authigenic quartz is consistent with burial temperatures greater than 80 °C (e.g., Walderhaug, 1994). Other features, such as the development of stylolites, are also consistent with alteration during burial and compaction.
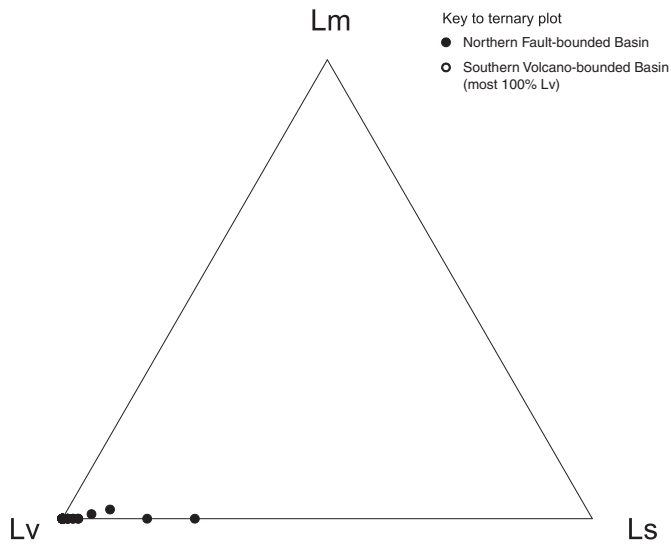
Fig. 3. Total quartz (Qt), feldspar (F), and lithic (L) ternary plot of Alisitos data. See Table 1 for formulae used in calculating QtFL percentages and Table 2 for the data plotted in this figure.
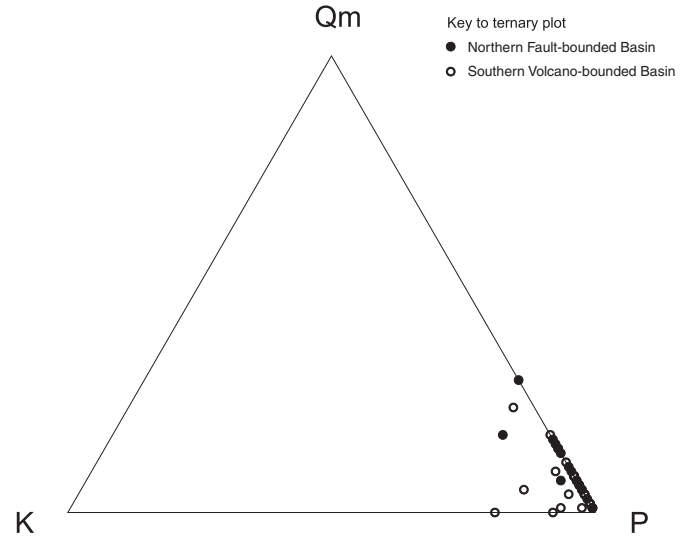
Fig. 5. Monocrystalline quartz (Qm), potassium feldspar (K), and plagioclase (P) ternary plot of Alisitos data. See Table 1 for formulae used in calculating QmKP percentages and Table 2 for the data plotted in this figure.
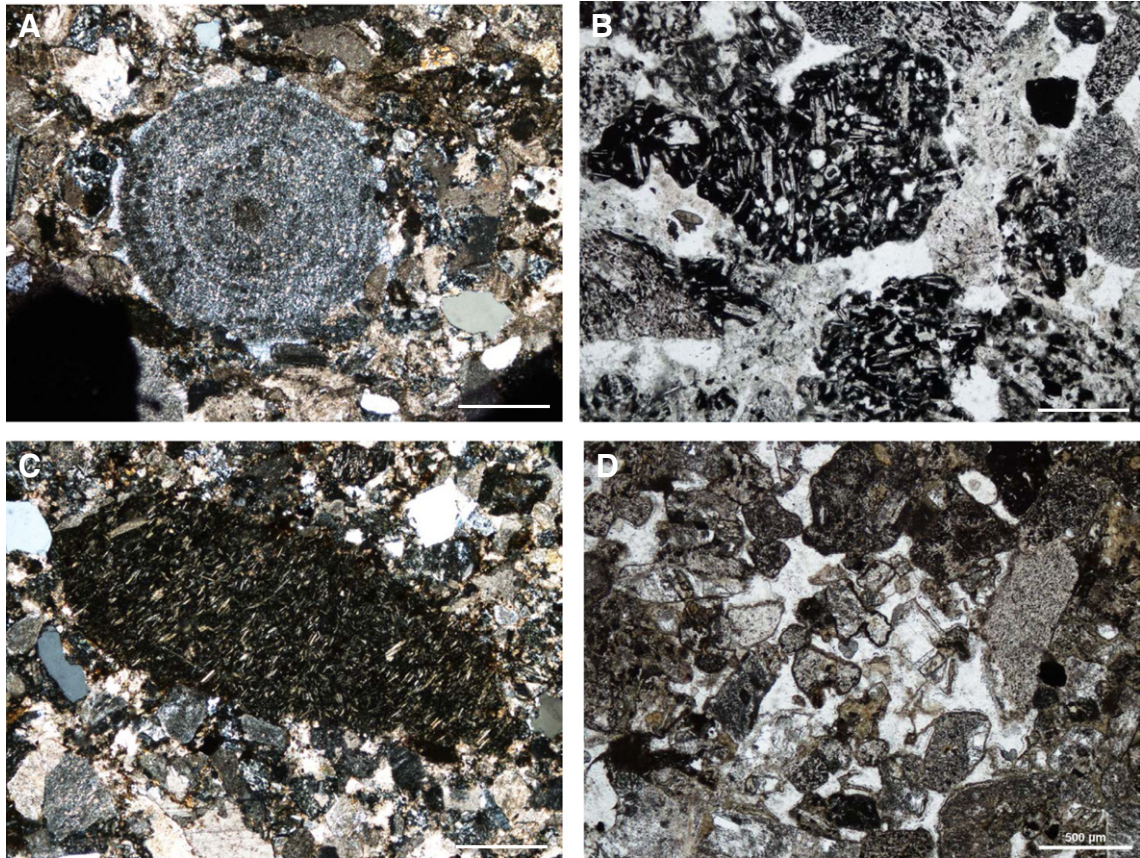
Fig. 4. Photomicrographs illustrating various grain types and textures in Alisitos samples. A. The field of view is dominated by the cross-section of an echinoid spine exhibiting near-unit extinction under crossed polars. Note the smaller rounded quartz grains in the lower right corner of the field of view and the pervasive carbonate cementation. This sample (248) is from the fault-bounded basin section. B. Grain-supported mix of more irregular black tachylitic basalt fragments with lathwork texture and smaller, more rounded microlitic fragments cemented by colorless zeolites and quartz. This sample (233) is from the fault-bounded basin section. C. The field of view contains a large rounded clast of microlitic glass with birefringent microlites and isotropic glass (black) as shown in this view with polars crossed. In plane light, the glass is tan in color. Surrounding grains include altered plagioclase and quartz set in carbonate cement. This sample (196) is from the volcano-bounded basin section. D. This volcaniclastic sandstone consists of rounded grains of intermediate to mafic composition. Under crossed polars, the colorless minerals filling interstitial areas can be identified as coarsely crystalline carbonate, and plagioclase phenocrysts are partly replaced by carbonate. This sample (182) is from the volcano-bounded basin. All scale bars are 50 microns in length.
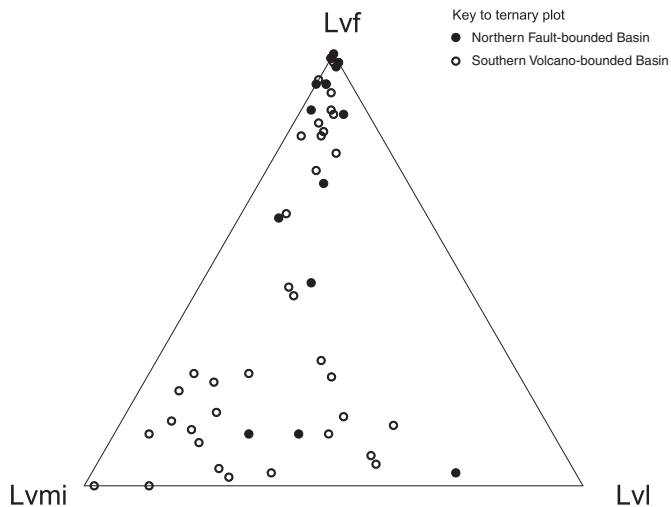
Fig. 6. Lithic ternary plot of Alisitos data illustrating the relative proportion of metamorphic (Lm), volcanic (Lv), and sedimentary (Ls) lithic fragments. See Table 1 for formulae used in calculating LmLvLs percentages and Table 2 for the data plotted in this figure.
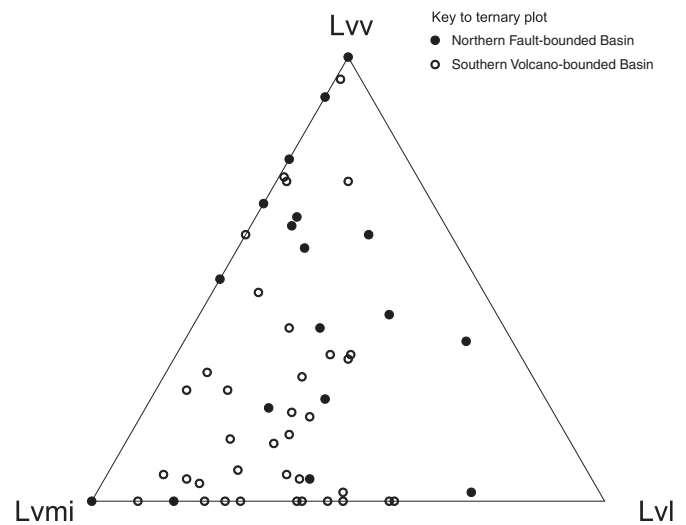

Fig. 8. Ternary plot illustrating the relative proportions of volcanic lithics with felsitic (Lvf), microlitic (Lvmi), and lathwork (Lvl) textures in the Alisitos samples. See Table 1 for formulae used in calculating Lvf-Lvmi-Lvl percentages and Table 2 for Alisitos data plotted in this figure.

6. Discussion

6.1. Relating compositional modes to facies

Previous work has shown that submarine explosive arc magmatism produces pyroclastic units dominated by angular vitric components (e.g., Izu–Bonin Arc; Marsaglia, 1992), whereas epiclastic sand derived from erosion of subaerial volcanic edifices has higher microlitic and lathwork proportions (e.g., Marsaglia, 1991; Marsaglia and Ingersoll, 1992; Caracciolo et al., 2011, 2012) and it is better rounded (Marsaglia, 1993). The Alisitos samples show a compositional range that encompasses both extremes (Figs. 8, 9), suggesting that they consist mainly of primary to redeposited pyroclastic debris, with lesser epiclastic products of physical and/or chemical weathering in coastal or stream environments; both types were potentially affected by littoral and shelf currents prior to deposition or transport into deeper water. Reworking is also indicated by the mixture of lithic textures observed in many samples, and the common presence of rounded volcanic grains (Fig. 4). Petrographic observations show that the northern fault-
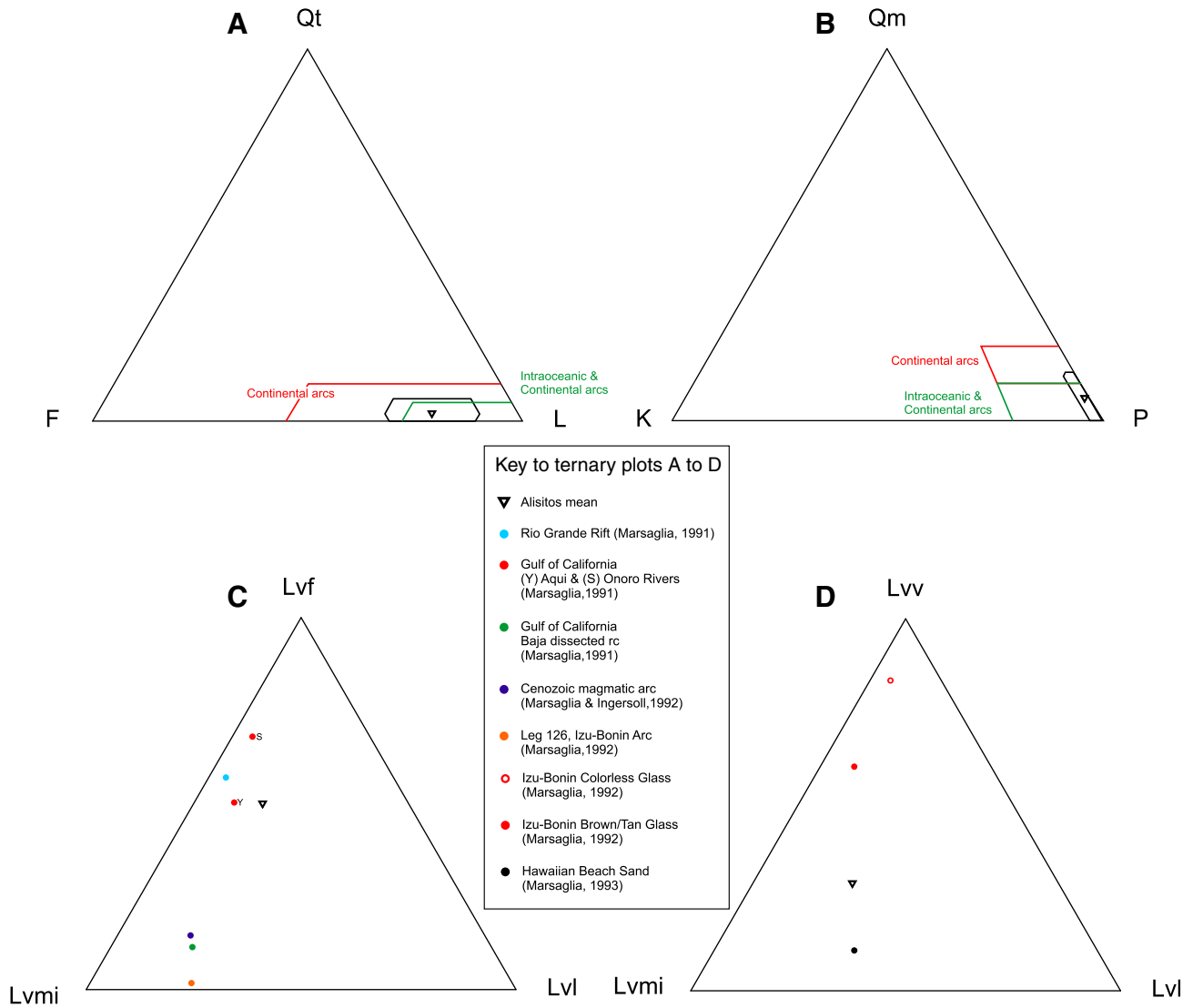
bounded basin section shows a progressive upsection increase in grain rounding and concomitant enrichment in monocrystalline grains, suggesting that after a volcanic eruption, tuffaceous sediments were progressively reworked through time. Recent detailed multibeam studies of the submarine part of the Anatahan volcanic complex in the Mariana Arc appear to show significant downslope reworking and likely mixing of arc-generated pyroclastic/volcaniclastic debris in associated basins (Chadwick et al., 2005). Such volcanic islands are also prone to high-energy wave erosion and reworking by ocean currents, for example, at Stromboli (e.g., Casalbore et al., 2010).

6.2. Relating compositional modes to basin type

Our data set allows for direct comparison of sand modal signatures of volcano-bounded shallow-marine vs. fault-bounded deep-marine arc basin fill along one segment of the Alisitos arc. The dominant volcanic lithic assemblages of microlitic (Lvmi) and lathwork (Lvl) grains in the southern volcano-bounded shallow-marine section (Figs. 6, 7) suggest a principal volcanic provenance from more crystalline lavas on the emergent volcanic edifices (but note that the primary pyroclastic flow deposits were not sampled). Very minor amounts of metamorphic (e.g., phyllite grains) and sedimentary lithic components present in a few samples within the northern fault-bounded deep-marine basin are consistent with its location in a fault-bounded basin, where metamorphic or sheared (fault gouge?) and sedimentary rocks are more likely to have been exposed along footwall margins. The northern fault-bounded, deep-marine-basin section appears to be, on average, richer in felsitic grains (Lvf) relative to the southern volcano-bounded shallow-marine section (Fig. 7) because these tuffs/tuffaceous sandstones are likely in large part the lateral equivalents of the massive pyroclastic flow deposits in the southern volcano-bounded shallow-marine section (which were not sampled). The northern fault-bounded deep-marine basin includes many more samples with high microlitic volcanic lithic content (Fig. 7). The higher microlitic content is consistent with a main source of more intermediate to mafic composition (see Marsaglia, 1993).

6.3. Comparison to other magmatic arcs

In general, detrital modes of Alisitos arc sand are similar to those from other modern and ancient magmatic arcs. Marsaglia and Ingersoll (1992) plotted mean QtFL values for modern magmatic arcs

Fig. 7. Ternary plot illustrating the relative proportion of volcanic lithics with vitric (Lvv), microlitic (Lvmi), and lathwork (Lvl) textures in the Alisitos samples. See Table 1 for formulae used in calculating Lvv-Lvmi-Lvl percentages and Table 2 for Alisitos data plotted in this figure.

Fig. 9. Ternary plots of Alisitos samples illustrating the proportions of A) Qt (total quartz), F (feldspar), and L (lithic fragments) with fields from Marsaglia and Ingersoll (1992) for comparison; B) Qm (monocrystalline quartz), K (potassium feldspar), and P (plagioclase) with fields from Marsaglia and Ingersoll (1992) for comparison; C) Lvv (vitric), Lvmi (microlitic), and Lvl (lathwork) volcanic lithics with mean values from other publications for comparison as noted. D) Lvf (felsitic), Lvmi (microlitic), and Lvl (lathwork) volcanic lithics with mean values from other publications for comparison as noted.

and showed that the compositional fields for continental and micro-continental arcs overlapped, but continental/micro-continental arcs could sometimes be discriminated from intraoceanic arcs in terms of their higher average quartz (QtFL%Q > 5) and/or feldspar (QtFL%F > 25) proportions. The mean Alisitos composition falls in the field of overlap and cannot be unequivocally assigned as intraoceanic or continental (Fig. 8). This may be because volcanic quartz is present, consistent with the presence of silicic pyroclastic volcanic rocks in oceanic arcs undergoing extension/rifting, both modern (e.g., Izu arc) and ancient (Alisitos arc; see discussion in Busby et al., 2006).

The mean monomineralic proportions (Fig. 8) also plot in the mixed intraoceanic to continental arc QmKP field of Marsaglia and Ingersoll (1992). Some Alisitos samples are enriched in felsitic fragments (Fig. 9). The high proportion of fragments with felsitic texture, a devitrification texture comprising microcrystalline feldspar and quartz, may be related to the slower cooling rate of flows and ignimbrites in subaerial settings vs. rapid quenching in submarine settings that produces vitric textures. For example, only traces of felsitic components were found in extensional/rifting intraoceanic arcs where the volcanic centers are largely submarine calderas (e.g., Izu–Bonin and Marianas;

Marsaglia, 1991; Marsaglia and Devaney, 1995), and moderate proportions in sands associated with modern magmatic arcs in general (Marsaglia and Ingersoll, 1992). The highest percentages occur in sediments derived from dissected subaerial felsic volcanic centers in the Sierra Madre Occidental of Mexico, an extensional arc (Marsaglia, 1991). The higher felsitic lithic content of the Alisitos samples is consistent with an extensional oceanic arc with a subaerial central edifice, as documented previously by Busby et al. (2006).

The Early Cretaceous Alisitos extensional oceanic arc shows compositional ranges similar to those of the Jurassic Gran Canon strongly extensional oceanic arc-ophiolite terrane, from felsic to mafic petrofacies (Critelli et al., 2002). Within Phase 1 (extensional arc) of the Alisitos arc, there are no distinct upsection compositional trends, but Phase 2 of the Alisitos arc (rifted arc) is similar to the second arc rifting event recorded in the Gran Canon Formation (described above), with its mafic lavas and silicic pyroclastic flow deposits. There is slightly higher quartz content at the top of the volcano-bounded basin section and in the middle of the fault-bounded basin section (Table 2), but these trends could be related to local variations in eruptive products or reworking.

7. Conclusions

The undeformed and unmetamorphosed exposures of the Rosario segment of the Alisitos extensional oceanic arc provides an excellent opportunity to study detrital modes of proximal arc facies, in a volcano-bounded shallow-marine basin and a fault-bounded deep-marine basin on either side of a central subaerial edifice. In modern settings, these proximal facies are not well studied due to drilling difficulties, and in many accreted arcs, the rocks are too deformed and metamorphosed for stratigraphic and modal analysis. We show here that despite differences in basin types and associated transport and depositional processes, detrital modes do not vary significantly, suggesting that proximal arc-axis basins of varying types around a single major subaerial edifice provide a faithful record of volcanic trends in the arc segment, regardless of transport and depositional processes. Only subtle compositional variations of grain types might be related to basin type, including (1) input (albeit sparse) from footwall scarps in the fault-bounded basin and (2) higher degree of crystallinity of volcanic lithics in the volcano-bounded basin, related to local variations in source rocks on the central subaerial edifice, greater reworking on the flanks of the shallow-marine volcano-bounded basin, or differences in the contribution of subaerially vs. subaqueously erupted debris.

References

Alsleben, H., Wetmore, P.H., Gehrels, G.E., Paterson, S.R., 2012. Detrital zircon ages in Palaeozoic and Mesozoic basement assemblages of the Peninsular Ranges batholith, Baja California, Mexico: constraints for depositional ages and provenance. International Geology Review 54, 93–110.

Busby, C., 2004. Continental growth at convergent margins facing large ocean basins: a case study from Mesozoic convergent-margin basins of Baja California, Mexico. Tectonophysics 392, 241–277.

Busby, C.J., Boles, J.R., 1988. Geologic field guide to selected Cretaceous forearc and intra-arc rocks of Baja California del Norte, Mexico. In: Weide, D.L., Faber, M.L. (Eds.), This extended land; geological journeys in the southern Basin and Range, pp. 311–330.

Busby, C., Fackler-Adams, B.N., Matinson, J., Deoreo, S., 2006. View of an intact oceanic arc, from surficial to mesozonal levels: Cretaceous Alisitos Arc, Baja California. Journal of Volcanology and Geothermal Research 149, 1–46.

Busby-Spera, C.J., 1988. Evolution of a Middle Jurassic back-arc basin, Cedros Island, Baja California: evidence from a marine volcaniclastic apron. Geological Society of America Bulletin 100, 218–233.

Caracciolo, L., Critelli, S., Innocenti, F., Kolios, N., Manetti, P., 2011. Unravelling provenance from Eocene–Oligocene sandstones of the Thrace Basin, North-east Greece. Sedimentology 58, 1988–2011.

Caracciolo, L., Von Eynatten, H., Tolosana-Delgado, R., Critelli, S., Manetti, P., Marchev, P., 2012. Petrological, geochemical, and statistical analysis of Eocene–Oligocene sandstones of the Western Thrace Basin, Greece and Bulgaria. Journal of Sedimentary Research 82, 482–498.

Casalbore, D., Romagnoli, C., Chiocci, F., Frezza, V., 2010. Morpho-sedimentary characteristics of the volcaniclastic apron around Stromboli volcano (Italy). Marine Geology 269, 132–148.

Cavazza, W., Caracciolo, L., Critelli, S., D'Atri, A., Zuffa, G.G., 2013. Petrostratigraphic evolution of the Thrace Basin (Bulgaria, Greece, Turkey) within the context of Eocene–Oligocene post-collisional evolution of the Vardar–Izmir-Ankara suture zone. Geodinamica Acta 26, 12–26.

Centeno-Garcia, E., Busby, C., Busby, M., Gehrels, G., 2011. Evolution of the Guerrero composite terrane along the Mexican margin, from extensional fringing arc to contractional continental arc. Geological Society of America Bulletin 123, 1776–1797.

Chadwick Jr., W.W., Embley, R.W., Johnson, P.D., Merle, S.G., Ristau, S., Bobbitt, A., 2005. The submarine flanks of Anatahan Volcano, commonwealth of the Northern Marianas. Journal of Volcanology and Geothermal Research 146, 8–25.

Critelli, S., Ingersoll, R.V., 1995. Interpretation of neovolcanic versus palaeovolcanic sand grains; an example from Miocene deep-marine sandstone of the Topanga Group (Southern California). Sedimentology 42, 783–804.

Critelli, S., Marsaglia, K.M., Busby, C.J., 2002. Tectonic history of a Jurassic backarc-basin sequence (the Gran Canon formation, Cedros Island, Mexico), based on compositional modes of tuffaceous deposits. Geological Society of America Bulletin 114, 515–527.

Dickinson, W.R., 1970. Interpreting detrital modes of graywacke and arkose. Journal of Sedimentary Petrology 40, 695–707.

Dickinson, W.R., Lawton, T., 2001. Carboniferous to Cretaceous assembly and fragmentation of Mexico. Geological Society of America Bulletin 113, 1142–1160.

Dickinson, W.R., Suczek, C.A., 1979. Plate tectonics and sandstone compositions. American Association of Petroleum Geologists Bulletin 63, 2164–2183.

Dickinson, W.R., Beard, L.S., Brackenridge, G.R., Erjavec, J.L., Fergusen, R.C., Inman, K.F., Knepp, R.A., Lindenberg, F.A., Ryberg, P.T., 1983. Provenance of North American Phanerozoic sandstones in relation to tectonic setting. Geological Society of America Bulletin 94, 222–235.

Fackler-Adams, B.N., Busby, C.J., 1998. Structural and stratigraphic evolution of extensional oceanic arcs. Geology 26, 735–738.

Ingersoll, R.V., Bullard, T.F., Ford, R.L., Grimm, J.P., Pickle, J.D., Sares, S.W., 1984. The effect of grain size on detrital modes: a test of the Gazzi–Dickinson point-counting method. Journal of Sedimentary Petrology 54, 103–116.

Marsaglia, K.M., 1991. Provenance of sands and sandstones from the Gulf of California, a rifted continental arc. In: Fisher, R.V., Smith, G.A. (Eds.), Sedimentation in Volcanic Settings. SEPM Special Publication 45, pp. 237–248.

Marsaglia, K.M., 1992. Petrography and provenance of volcaniclastic sands recovered from the Izu–Bonin arc, Leg 126. Proceedings of the Ocean Drilling Program, Scientific Results 126, 139–154.

Marsaglia, K.M., 1993. Basaltic Island Sand Provenance. In: Johnsson, M.J., Basu, A. (Eds.), Processes controlling the composition of clastic sediments. Geological Society of America Special Paper 284, pp. 41–65.

Marsaglia, K.M., 1995. Interarc and backarc basins Chapter 8 In: Busby, C., Ingersoll, R.V. (Eds.), Tectonics of Sedimentary Basins. Blackwell, pp. 299–329.

Marsaglia, K.M., Devaney, K.A., 1995. Tectonic and magmatic controls on backarc basin sedimentation: the Mariana Region re-examined. In: Taylor, B. (Ed.), Backarc Basins: Tectonics and Magmatism. Plenum, New York, NY, pp. 497–520.

Marsaglia, K.M., Ingersoll, R.V., 1992. Compositional trends in arc-related, deep-marine sand and sandstone: a reassessment of magmatic-arc provenance. Geological Society of America Bulletin 104, 1637–1649.

Marsaglia, K.M., Tazaki, K., 1992. Diagenetic trends in Leg 126 sandstones. Proceedings of the Ocean Drilling Program, Scientific Results 126, 125–138.

Morton, D.M., Miller, F.K. (Eds.), 2014. Peninsular Ranges Batholith, Baja California and Southern California. Geological Society of America Memoir 211, p. 758.

Perri, F., Critelli, S., Cavalcante, F., Mongelli, G., Sonnino, M., Dominici, R., De Rosa, R., 2012. Provenance signatures for the Miocene volcaniclastic succession of the Tufiti di Tusa Formation, southern Apennines, Italy. Geological Magazine 149, 423–442.

Silver, L.T., Stehli, F.G., Allen, C.R., 1963. Lower Cretaceous prebatholithic rocks of northern Baja California, Mexico. American Association of Petroleum Geologists Bulletin 47, 2054–2059.

Smith, G.A., Landis, C.A., 1995. Intra-arc Basins. In: Busby, C.J., Ingersoll, R.V. (Eds.), Tectonics of Sedimentary Basins. Blackwell, Cambridge, Mass, pp. 263–298.

Taylor, B., and 24 others, 1990. Proceedings of the Ocean Drilling Program, Initial reports, Leg 126, Sites 787– 793, Bonin arc-trench system: College Station, Texas, Ocean Drilling Program 126, 1002 p.

Walderhaug, O., 1994. Precipitation rates for quartz cement in sandstones determined by fluid-inclusion microthermometry and temperature-history modeling. Journal of Sedimentary Research A64, 324–333.

Wetmore, P.H., 2002. Tectonic implications for the along-strike variation of the Peninsular Ranges Batholith, Southern and Baja California. Geology 30, 247–250.

Wetmore, P.H., Herzig, C., Asleben, H., Sutherland, M., Schmidt, K.L., Schultz, P.W., Paterson, S.R., 2003. Mesozoic tectonic evolution of the Peninsula Ranges of southern and Baja California. In: Johnson, S.E., et al. (Eds.), Tectonic evolution of northeastern Mexico and the southwestern USA. Geological Society of America Special Paper 374, pp. 93–116.